*Journal of the Earth Simulator*, Volume 8, November 2007, 3–11

# Seasonal and Intra-Seasonal Variability of Chlorophyll-a in the North Pacific: Model and Satellite data

Yoshikazu Sasai[1]*, Kosei Sasaoka[1], Hideharu Sasaki[2], and Akio Ishida[1, 3]

[1] *Frontier Research Center for Global Change, Japan Agency for Marine-Earth Science and Technology, 3173-25, Showa-machi, Kanazawa-ku, Yokohama, 236-0001, Japan*
[2] *The Earth Simulator Center, Japan Agency for Marine-Earth Science and Technology, 3173-25, Showa-machi, Kanazawa-ku, Yokohama, 236-0001, Japan*
[3] *Institute of Observational Research for Global Change, Japan Agency for Marine-Earth Science and Technology, 2-15, Natsushima-cho, Yokosuka-city, Kanagawa, 237-0061, Japan*

(Received January 12, 2007; Revised manuscript accepted May 8, 2007)

**Abstract** The seasonal and intra-seasonal variability of chlorophyll-a in the North Pacific is investigate using an ocean color satellite data and a simplified four-component ecosystem model embedded in an eddy-resolving ocean general circulation model. The model captures the realistic seasonal variability of chlorophyll-a distribution associated with the mesoscale eddy activities, sub-mesoscale front variability, western boundary current (Kuroshio), and upwelling. The variability of basin-wide high chlorophyll-a zone between subarctic and subtropical gyres is clearly reproduced in the model. The Kuroshio Extension region exhibits the several time and spatial scale variability. In spring, the westward anticyclonic eddy at the south of Kuroshio Extension deepens the nutricline in the subsurface layer and reduces the biological production during the few days. The generated many anticyclonic and cyclonic eddies along the Kuroshio affect the ecosystem dynamics. The biological production responds to the uplift and depress of nutricline with the variability of mesoscale physical phenomena.

**Keywords**: chlorophyll-a, seasonal variability, high-resolution OGCM, ocean color satellite data, and North Pacific

## 1. Introduction

Distribution of surface chlorophyll-a (chl-a) concentrations in the global ocean is measured by the ocean color sensors since in the last few decades, such as the Coastal Zone Color Scanner (CZCS), Ocean Color and Temperature Scanner (OCTS), the Sea-viewing Wide Field of view Sensor (SeaWiFS), Global Imager (GLI) and the Moderate Resolution Imaging Spectroradiometer (MODIS). Using these ocean color satellite data, the temporal and spatial variations of chl-a distribution in the North Pacific are discussed [e.g., 1, 2, 3]. These ocean color satellites capture the temporal and spatial variations in the surface marine biology, which is connected to changes in the physical environment. The effect of physical processes, which are transport and mixing, is reflected in the measured surface chl-a concentrations. Especially, in the western boundary regions, chl-a picture shows the pattern correlated with the western boundary current, the meso-scale eddies, and fine-scale fronts and filaments.

The condition for biological production depends on the major physical factors. Light is one controlling factor for biological production. Ocean transport and mixing processes (e.g., vertical advection, mixing, and convection, three-dimensional circulation) supply high nutrients from the deep layer into the euphotic zone. In winter season, the deepening of the mixed layer in mid-latitude and high-latitude regions supplies high nutrients from deep to the surface ocean. These features largely determine what types of phytoplankton develop and how much biological production occurs in the world ocean.

Currently, high-resolution ocean models are used to investigate the interplay of marine biology and physical processes in the basin scales [e.g., 4, 5, 6]. In the North Atlantic, the basin wide simulation of ecosystem using high-resolution models has been performed [4, 7, 8]. The horizontal grid spacing is from 1/3˚ (eddy-permitting) to 1/10˚ (eddy-resolving). The eddy enhancement of export production over the basin scale has been examined using

* ***Corresponding author***: *Yoshikazu Sasai, Frontier Research Center for Global Change, Japan Agency for Marine-Earth Science and Technology, 3173-25, Showa-machi, Kanazawa-ku, Yokohama, 236-0001, Japan, E-mail: ysasai@jamstec.go.jp*

a simple four-component nitrate-phytoplankton-zooplankton-detritus (NPZD) ecosystem model coupled with an eddy-permitting (1/3˚) resolution model [4, 7, 8] and an eddy-resolving (1/9˚) model [5]. Eddy-permitting and eddy-resolving models improved the model physics and clearly reproduced the aspect of seasonal cycle of surface chl-a, especially the spatial pattern in mid- and high-latitudes and in coastal upwelling regions [4, 5]. By increasing horizontal resolution, the enhancement of export production is principally achieved through an eddy vertical transfer of nutrients around the Gulf Stream and an eddy horizontal transfer along the flanks of the subtropical gyre [5]. For the North Pacific, [6] showed the annual cycle of temperature, nitrate, and phytoplankton in the upper ocean using a global eddy-resolving (1/10˚) coupled physical-biological model. [9] also pointed out the improvement of biological fields near-shore region with the realistic wind forcing.

In this study, we use the spatial and temporal high-resolution of surface chl-a data provided by the ocean color sensor and the global eddy-resolving coupled physical-biological model to investigate the surface seasonal variability and vertical structure of chl-a distribution in the North Pacific. By combining a fine resolution satellite data with a high-resolution coupled physical-biological model, it is possible to investigate the vertical structure of chl-a distribution in the ocean interior. We also examine the performance and accuracy of model compared with ocean color satellite data.

## 2. Model Description and Satellite data

We have used an eddy-resolving ocean model for the Earth Simulator (OFES) [10], which is based on the Geophysical Fluid Dynamics Laboratory's Modular Ocean Model (MOM3) [11]. The domain covers from 75˚S to 75˚N. The horizontal resolution is 0.1˚. The vertical levels are 54, with varying distance between the levels from 5 m at the surface to 330 m at the maximum depth of 6065 m. The model topography is constructed from the 1/30˚ bathymetry dataset created by the OCCAM Project at the Southampton Oceanography Center.

The ocean is forced at the sea surface by seasonally varying climatological boundary conditions of temperature, salinity, and wind stress. Monthly mean wind stresses, averaged from 1950 to 1999 from the National Centers for Environmental Prediction/National Center for Atmospheric Research (NCEP/NCAR) reanalysis data, are used for the climatological seasonal integration. The surface heat flux is calculated by the same bulk formula as in Rosati and Miyakoda [12], using the monthly mean value from the NCEP/NCAR reanalysis outputs for the necessary data sets. The precipitation rate from the same NCEP/NCAR reanalysis data is used for the fresh water flux. Sea surface salinity is restored to the monthly mean climatological value of the World Ocean Atlas 1998. The model is integrated for 50 years from the annual mean temperature and salinity fields without motion [10]. After integration of 50-year periods, the model is driven by the daily mean NCEP/NCAR reanalysis from 1950 to 1998 [13].

The marine ecosystem model is a simple nitrogen-based NPZD pelagic model [8]. The evolution of any biological tracer concentration in the OFES is governed by an advection-diffusion equation with the source and sink terms. The source and sink terms are biological activities [6]. The phytoplankton growth rate depends on the light and nitrate concentration. The light is the NCEP/NCAR daily mean shortwave radiation. To establish the stable pattern of biological system, the biological model coupled with the evolving of physical fields is integrated over a 5-year period under the climatological mean forcing. The variability of biological fields has no feedback on the physical fields. The biological fields at the last are used as the initial condition. The initial condition of physical fields is from the last of 1998 (the end of NCEP/NCAR daily forcing run). The coupled model is driven by the daily mean surface wind stress data of Quick Scatterometer (QSCAT) satellite and atmospheric daily mean data (heat and salinity fluxes) of NCEP/NCAR reanalysis [13] from 1999 to 2004. The QSCAT data is from Japanese Ocean Flux data sets with Use of Remote sensing Observations (J-OFURO) [14] product. We have used a daily mean product, which is constructed over almost the whole ocean on each 1.0 grid spacing [15].

The temporal and spatial variability of chl-a in this study region was investigated using SeaWiFS (Ver.5) data. SeaWiFS data for 8-days and monthly composite global standard mapped images (SMI) (January 2004 to December 2004) were obtained from NASA GSFC's Ocean Color Web Site (http://oceancolor.gsfc.nasa.gov ). Both monthly and 8-days data sets have a spatial resolution of about 9 km. SeaWiFS images were remapped onto 0.1 degree grid to match with the model horizontal resolution.

All SeaWiFS images were processed with the SeaDAS Version 5.0 developed by NASA (http://seadas.gsfc.nasa.gov/). To analyze the time-series variability of chl-a distribution at the two stations, we used mean values of 1 degree by 1 degree squared box derived from SeaWiFS data using IDL (Interactive Data Language, Research Systems Inc.) software package.

## 3. Results

The marine ecosystem model embedded in an eddy-resolving ocean circulation model has been performed on the Earth Simulator. A stable pattern of the simulated sea-

sonal-cycle of biological fields is reached after the first coupled year. Results are presented for the last one-year period (atmosphere forcing year is 2004). We have examined the performance and accuracy of simulated marine biology compared with ocean color satellite data.

## 3.1 Seasonal and intra-seasonal variability of chlorophyll-a in the North Pacific

### 3.1.1 Horizontal distribution

Seasonal variability of surface chl-a concentrations in the North Pacific is shown in Figure 1. The simulated phytoplankton concentration (mmol $m^{-3}$) is converted to chlorophyll concentration using a ratio of 1.59 g chlorophyll per mol nitrogen. Qualitatively, simulated chl-a distribution has represented the seasonal variability, with low concentrations in the subtropical gyre and high concentrations in the upwelling, the Kuroshio and Kuroshio Extension regions, and subpolar gyre. In the western boundary region current regions, chl-a distribution has a very sharp pattern because of the influence of Kuroshio meander and frontal structure in both model and SeaWiFS image.

Using an eddy-resolving (horizontal resolution is 0.1˚) ocean circulation model, the ocean model can capture the realistic meso-scale phenomena, such as eddy, front, filament, and upwelling [10] and represent the realistic chl-a distribution. In the open ocean, the simulated chl-a concentration (2.0 mg $m^{-3}$) is higher than the SeaWiFS image (0.8 mg $m^{-3}$) during any season. In the coastal and marginal seas, the simulated chl-a concentration (< 5.0 mg $m^{-3}$) is lower than the SeaWiFS image (> 10.0 mg $m^{-3}$).

In winter (January and February), the model is clearly reproduced the high chl-a zone (HCZ) between 30˚N and 45˚N latitude (Figures 1.b.1 and 1.b.2). We have defined the HCZ as a chl-a concentration over 0.2 mg $m^{-3}$ between the subtropical and subarctic gyres. The ocean color satellites also show this feature (Figures 1.a.1 and 1.a.2). The HCZ is over 8000 km long and seasonally migrates north and south about 1000 km [16]. In the eastern North Pacific (from 180˚ to 120˚W), the simulated chl-a concentrations (0.4 – 0.8 mg $m^{-3}$) are larger than the SeaWiFS image (0.2 – 0.4 mg $m^{-3}$).

In spring (March - June), the simulated chl-a concentrations (0.8 – 1.0 mg $m^{-3}$) are higher than the SeaWiFS image (0.2 – 0.4 mg $m^{-3}$) except the coastal regions, marginal seas and the Kuroshio and Kuroshio Extension

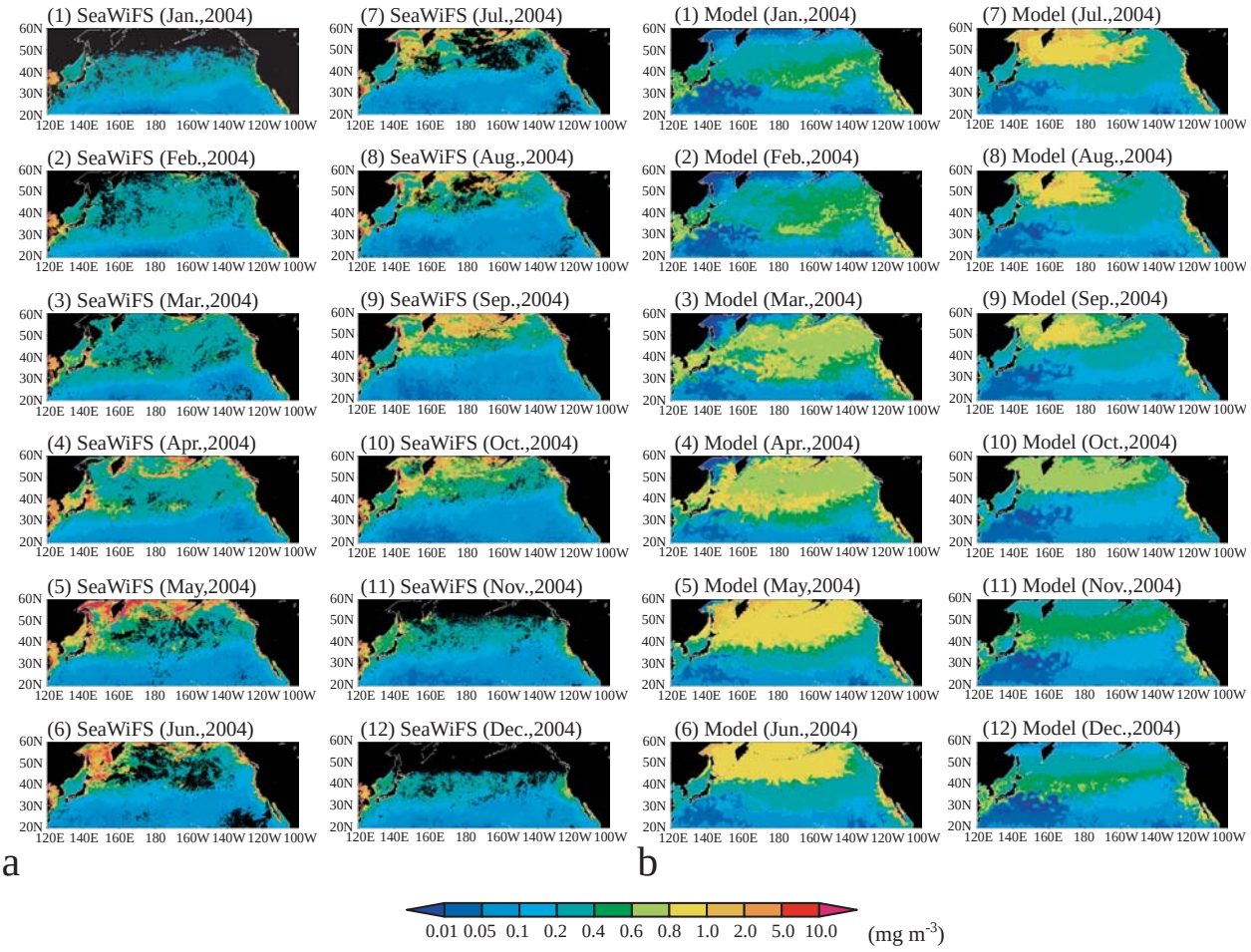


**Fig. 1** Distribution of surface chl-a concentration (mg $m^{-3}$) in 2004: (a) SeaWiFS satellite image, and (b) Model.

regions. In the coastal regions and marginal seas, the model (< 2.0 mg $m^{-3}$) is lower than the SeaWiFS (> 5.0 mg $m^{-3}$). In the Kuroshio and Kuroshio Extension regions, the distribution of chl-a influenced by the physical phenomena (eddy, front, and boundary current) is clearly reproduced in the model. The timing of spring bloom in the model is one or two months earlier than the SeaWiFS image, especially off the coast of Sanriku (northern part of Honshu Island), the Sea of Japan, and the Sea of Okhotsk. The SeaWiFS images capture the temporal pattern of spring bloom around the Japan (Figures 1.a.3, 1.a.4, and 1.a.5) [2, 3]. In the eastern subarctic Pacific, the chl-a concentration is lower than the western part in the ship and satellite observations [e.g., 1, 17], and the seasonal variability is not clearly shown. The difference in the biological productivity in the eastern and western subarctic Pacific is attributed the differences of biological structures, the nutrient input by the winter mixing, and the iron supply [18]. In the model, the distribution of chl-a concentration is uniform in the east and west in the north of 40˚N. Photosynthesis in the model is a function of light, temperature, and nitrate concentration. The light data uses the NCEP/NCAR daily mean shortwave radiation. In the biological model equation, the light is a parameterized as a photosynthetically active radiation and variable day length calculated from astronomical parameters. The seasonal variability of physical fields including a temperature and mixed layer depth is well reproduced in the OFES [19, 20]. The nutrient supply by the physical processes may not match for the biological activities. The biological model may not sufficiently represent the timing of spring bloom and phytoplankton growth rate. The biological model also does not include the iron limitation process and the phytoplankton species and size.

In summer (July - September), the pattern of simulated chl-a concentration is close to the SeaWiFS images pattern (Figures 1.a.7-1.a.9, and 1.b.7-1.b.9). In the model, the high chl-a area reduces with time. The satellite image captures the fall bloom (September) in the Sea of Okhotsk and the Bering Sea (Figure 1.a.9) [e.g., 2, 3]. The model may not reproduce the timing of fall bloom.

In fall (October - December), the zonal gradient of HCZ goes southward with moving the right condition (light intensity, temperature, and nitrate concentration) area for the biological production (Figures 1.b.10, 1.b.11, and 1.b.12). The satellite image could not show in the northern area, however the satellite also captures the HCZ feature (Figures 1.a.10, 1.a.11, and 1.a.12).

#### 3.1.2 Meridional and zonal sections

The comparison of chl-a concentration along the meridional and zonal sections is illustrated in Figure 2. We focus on the spring season variability (from April to June). Along the meridional section (150˚E), the SeaWiFS data shows the gradient of high chl-a concentration (0.2 – 0.7 mg $m^{-3}$) is moving northward. In April, the HCZ is between 30˚N and 35˚N (Figures 1.a.4 and 2a). In June, the HCZ moves at the 40˚N (Figures 1.a.6 and 2a). The difference of simulated chl-a between April and May is not clearly shown (Figure 2b). In June, the HCZ moves the northward of 40˚N. The model shows the low chl-a concentration between 30˚N and 35˚N influenced by the Kuroshio meander. The model could not reproduce the high chl-a concentration (> 3.0 mg $m^{-3}$) in the south of Okhotsk Sea (42˚N – 45˚N). In the zonal direction along 40˚N, the SeaWiFS data reveals the difference of chl-a concentration between east and west (Figure 2c). The chl-a concentration is high in the western side and is low in the eastern side. In June, the chl-a concentration is minimum as the HCZ moves northward. The simulated chl-a concentration is almost uniform in the zonal section and the spatial variability is small. In the California coast (125˚W – 120˚W), the model reproduces the high chl-a concentration with the coastal upwelling [9].

#### 3.1.3 Stations

The annual cycle of surface chl-a concentration at station A (40˚N, 150˚E) in the western subarctic gyre and station B (25˚N, 150˚E) in the western subtropical gyre (south of Kuroshio Extension) are shown in Figure 3. The western subarctic gyre has the large seasonal variability in physical, chemical, and biological parameters [e.g., 1, 21]. Both SeaWiFS and model values show the seasonal variability of surface chl-a concentration (Figure 3a). In the model, the peak of spring bloom (1.0 mg $m^{-3}$) is April and maintains until May. After spring bloom, the simulated chl-a concentration decreases until October. In November, the fall bloom (0.6 mg $m^{-3}$) occurs. The SeaWiFS data also shows the same peak of spring and fall blooms. In the western subtropical gyre (Figure 3b), the seasonal variability of Kuroshio is too large, however, biological production is too low compared with the subarctic region. Both SeaWiFS and model values show no seasonal variability of surface chl-a concentration in this region. The supply of nutrients is few during all season and the biological production does not increase.

### 3.2 Temporal variability in the Kuroshio Extension

The Kuroshio Extension region exhibits the several time and spatial scale variability [e.g., 19, 20]. Time-varying circulation associated with meso-scale eddies and submesoscale fronts is an energetic. The time-varying circulation supplies nutrient to the euphotic zone for biological production. Figure 4 shows a snapshot of chl-a distri-

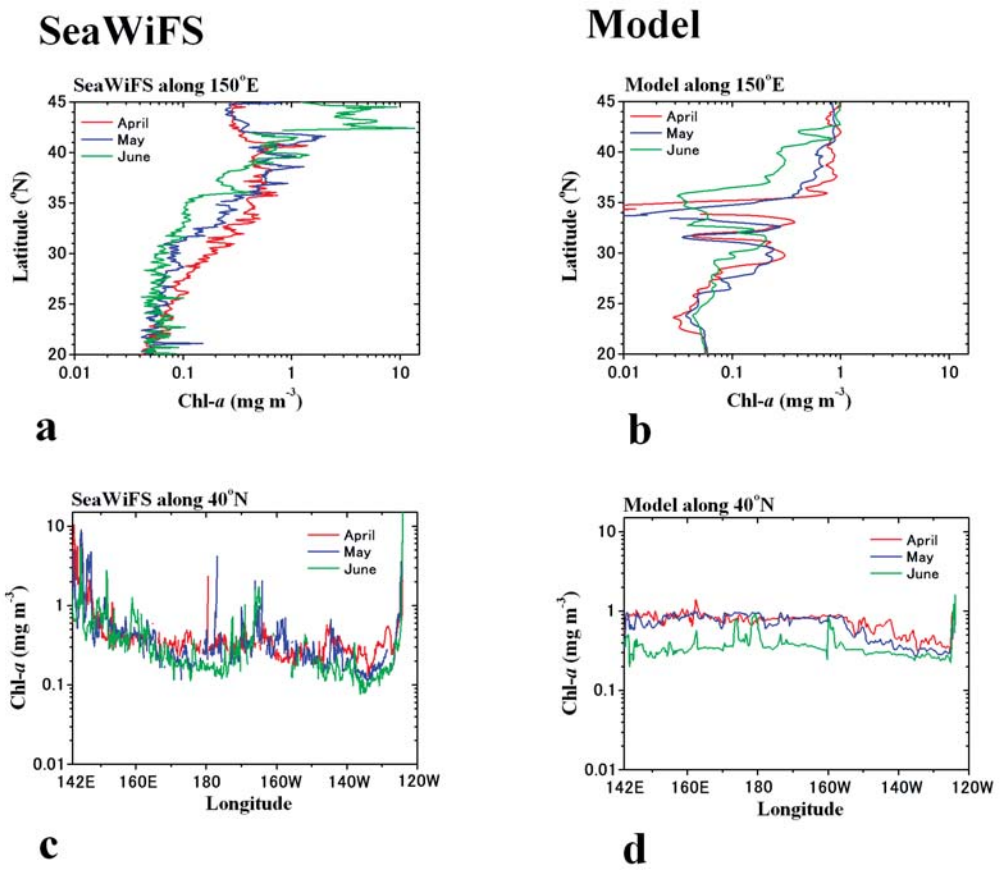


**Fig. 2** Surface chl-a concentration (mg $m^{-3}$) along (a)–(b) meridional (160˚E) and (c)–(d) zonal (40˚N) sections: (a), (c) SeaWiFS satellite image, and (b), (d) Model.

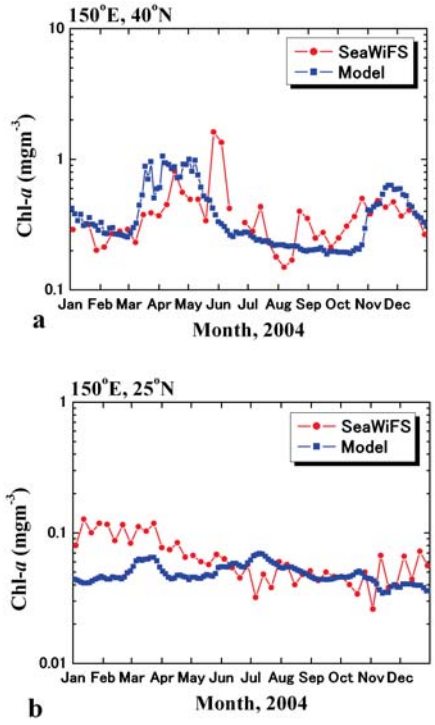


**Fig. 3** Time series of surface chl-a (mg $m^{-3}$) from SeaWiFS and model in 2004. Chl-a values are averaged with 1 degree by 1 degree square: (a) Station-A (150˚E, 40˚N), and (b) Station-B (150˚E, 25˚N).

bution in the Kuroshio Extension. Time intervals are 8-day of SeaWiFS (Figures 4.a.1, 4.b.1, and 4.c.1) and 3-day of model (Figures 4.a.2-4.a.4, 4.b.2-4.b.4, and 4.c.2-4c.4). This snapshots reveals signature of a range of physical processes: the meandering of the Kuroshio, the formation of meso-scale eddies and fine-scale frontal filaments drawn out between large-scale circulations. The model also reproduces a chl-a distribution influenced by the Kuroshio, meso-scale eddies and submesoscale fronts.

In general, the ocean color satellite has large cloud effects, especially in the North Pacific. In April, the SeaWiFS image relatively captures the pattern of chl-a distribution except for the cloud cover area (black color area in Figure 4.a.1, 4.a.2, and 4.a.3). By combining satellite data with a fine-resolution model results such as eddy-resolving (0.1˚) coupled physical biological model, it is possible to capture continuously the temporal variability of chl-a distribution associated with the physical processes including the cloud over area. In the open ocean, especially east of 150˚E, because the SeaWiFS does not measure the surface chl-a pattern along the Kuroshio Extension, by combining with the model, the whole pattern can be captured. At around 35˚N, the high chl-a north of Kursohio varies with the meandering of

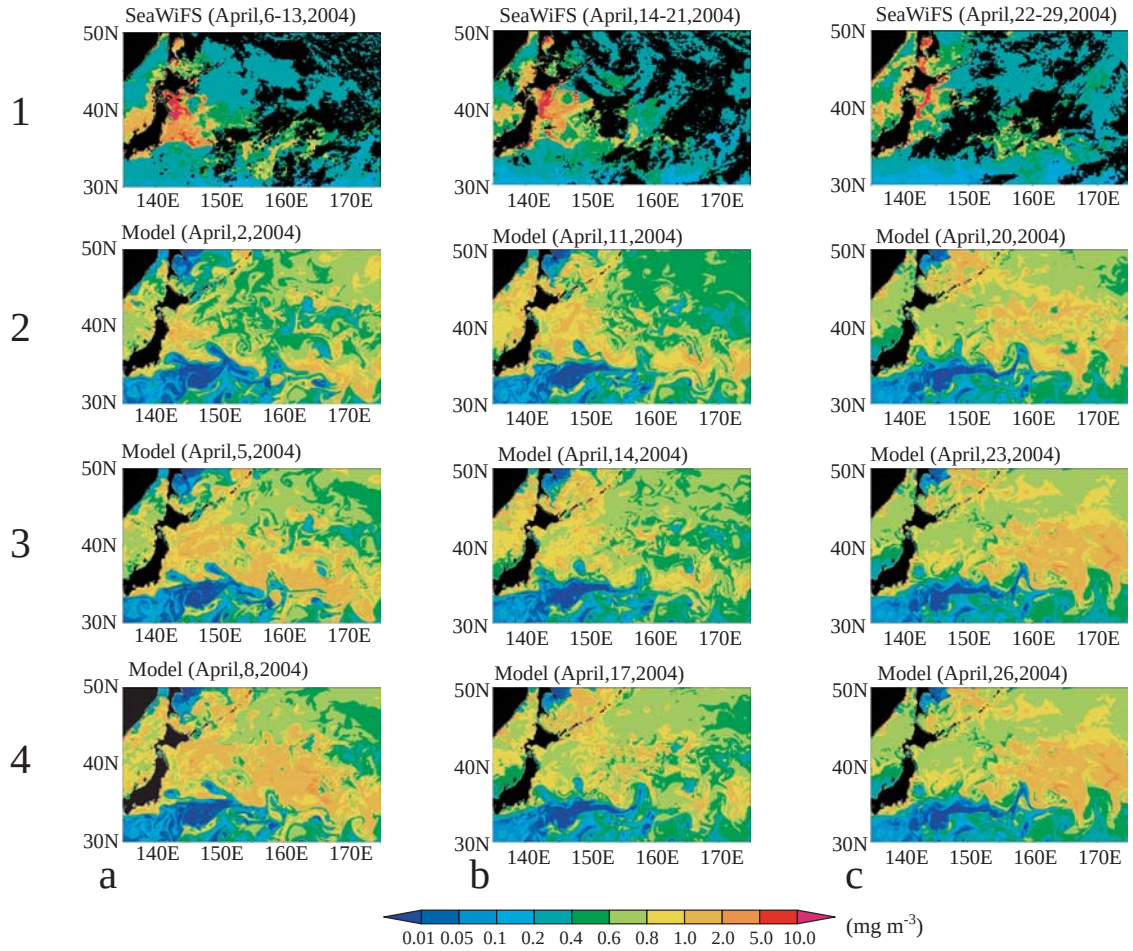


**Fig. 4** Temporal variation of surface chl-a concentration (mg $m^{-3}$) in April, 2004 in the Kuroshio Extension region from SeaWiFS and Model. Time resolutions are 8-days of SeaWiFS, and 3-day snapshot of Model.

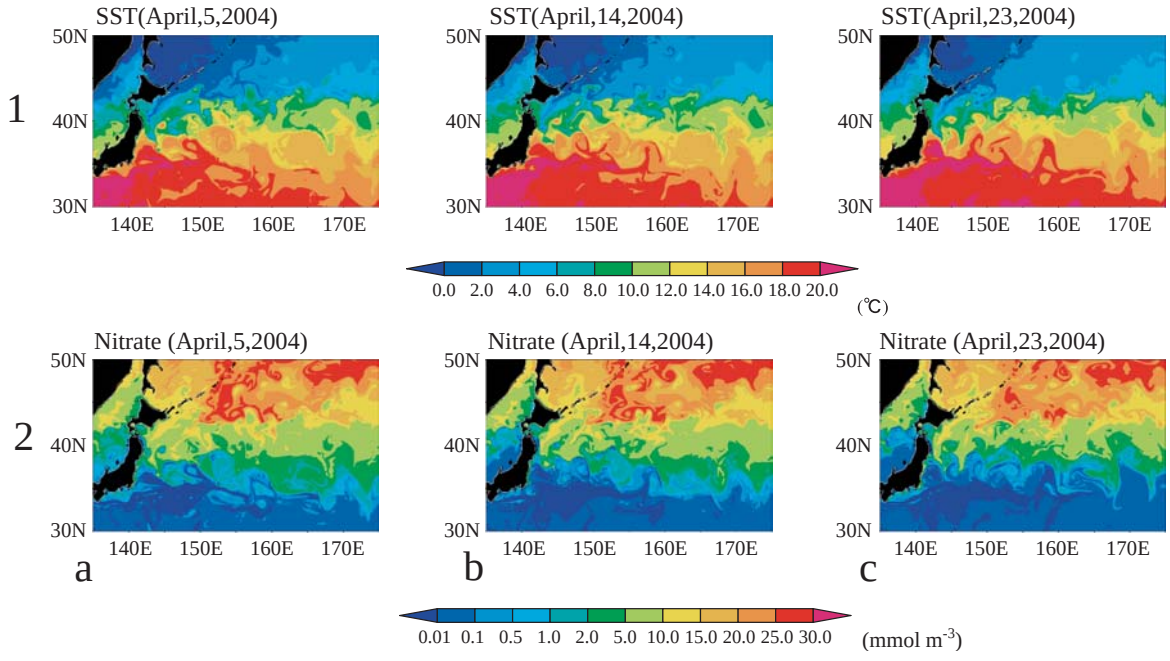


**Fig. 5** Distributions of sea surface temperature (˚C), and nitrate concentration (mmol $m^{-3}$) at the top layer from Model.

Kuroshio. In Figure 4c, SeaWiFS does not measure the high chl-a distribution along the Kuroshio depended on the cloud. In the same period of model, the time-varying chl-a distribution with the meandering of Kuroshio and meso-scale eddies is reproduced (Figures 4). The simulated chl-a distribution is mainly influenced by the seas surface temperature and nitrate concentration (Figure 5), particularly, south of 40˚N. The Kuroshio and meso-scale eddies in the model vary the nitrate distribution and affect the chl-a distribution through a rectified transfer of nitrate into the euphotic zone.

Figure 6 shows the temporal variability of chl-a distribution influenced by the anticyclonic eddy and meandering of Kuroshio along 145˚E. The surface simulated chl-a concentrations are close to the SeaFiWS data in the south of 32˚N and north of 36˚N. Between 32˚N and 36˚N, the simulated chl-a concentration is very low compared with the SeaWiFS data. The chl-a concentration is also very low through the water column (Figures 6.a.2, 6.b.2, and 6.c.2). The temperature increases and nitrate concentra-

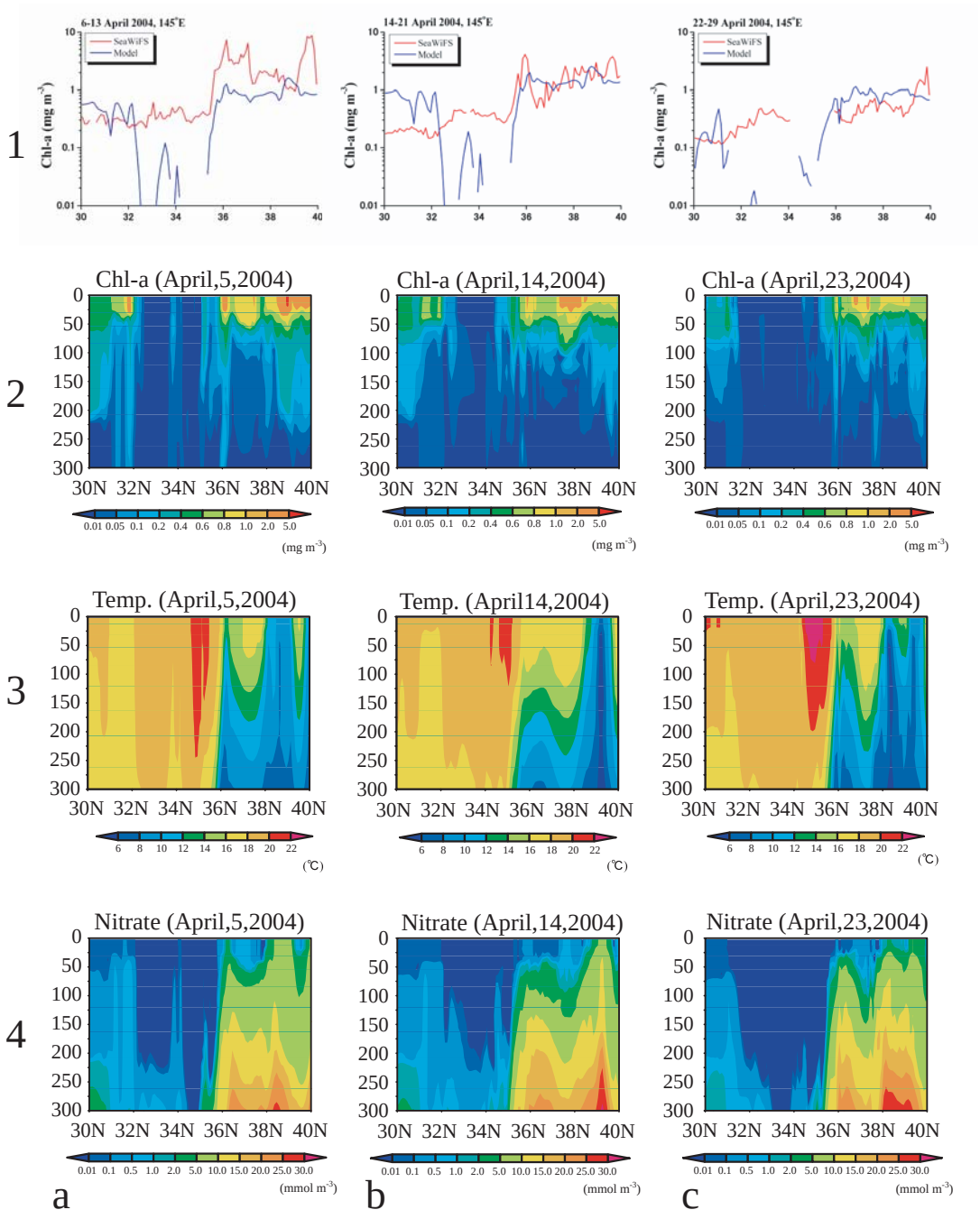


**Fig. 6** Surface chl-a concentration (mg $m^{-3}$) and vertical distributions of chl-a concentration (mg $m^{-3}$), temperature (˚C), and nitrate concentration (mmol $m^{-3}$) along 145˚E section from 30˚N to 40˚N in (a) April, 5, (b) April, 14, and (c) April, 23, 2004.

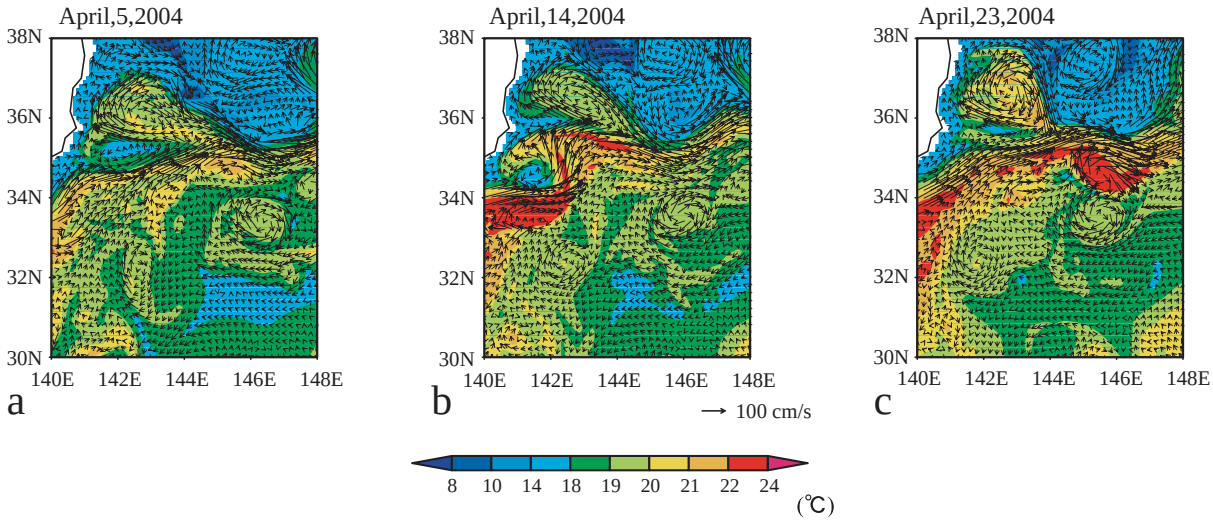


**Fig. 7** Meso-scale variability in the Kuroshio Extension in (a) April, 5, (b) April, 14, and (c) April, 23 in 2004. Vectors are horizontal velocities (cm $s^{-1}$) at 25 m depth. Color shade is temperature (˚C) at 25 m depth.

tion decreases with time (Figures 6.a.4, 6.b.4, and 6.c.4). The low simulated chl-a concentration between 32˚N and 36˚N is caused by the low nitrate concentration. In this region, light and temperature conditions are enough to the biological production. The biological production is mainly controlled by the nitrate concentration. The simulated nitrate concentration is much lower than the observation (April mean is about 2 mmol $m^{-3}$). The nitrate concentration in the transported Kuroshio water is underestimated in the model. The photosynthesis speed in the biological model may be faster than the nitrate supply speed by physical processes.

Horizontal distribution of subsurface temperature with velocity field in the model is shown in Figure 7. The meander is between 34˚N and 36˚N and the anticyclonic eddy (diameter is about 80 km) moves westward along 33˚N. On April 5th, the meander between 34˚N and 36˚N affects the chl-a concentration (Figures 6.a.2 and 7a). When the anticyclonic eddy comes from east (Figure 7c), low nitrate area deepens (Figure 6.c.4) and chl-a concentration in the inside of eddy decreases (Figure 6.c.2). Fine resolution observation such as satellite and model studies suggest that the nutrient supply by the small scale circulation (e.g.., meso-scale eddies and submesoscale fronts) supports significant fraction of biological production.

## 4. Summary

We have investigated the surface seasonal variability and the vertical structure of chl-a distribution in the North Pacific using a fine resolution scale satellite data and a global eddy-resolving coupled physical-biological ocean model. The model captures realistic variability of surface chl-a distribution associated with the meso-scale eddy activities, submesoscale front variability, western boundary current (Kuroshio), and upwelling. The basin-wide high chl-a zone between two major gyres (subarctic and subtropical) is clearly reproduced in the model. The transition zone chl-a front is important frontal habitat zonally spanning the North Pacific [16]. We have focused on the small time scale variability in the Kuroshio Extension. In spring season, the westward anticyclonic eddy at the south of Kuroshio Extension deepens the nutricline in the subsurface layer and reduces the biological production. The time-varying circulation such as mesoscale eddies, fronts, and meander modifies the biological field. The generated many anticyclonic and cyclonic eddies along the Kuroshio, which is a strong western boundary current, affects the ecosystem dynamics. These eddies uplift and depress the nutricline in the subsurface layer and the biological production responds to the nitrate concentration.

It is difficult to examine the small time-scale variability (from few days to months) of chl-a distribution using an ocean satellite data. Because there is a large effect of cloud cover, especially in the North Pacific. The model provides the high spatial and temporal resolution data. By combining a fine resolution satellite data with a high-resolution coupled physical-biological model, it is possible to investigate the effects of relevant of physical dynamics detail, such as the frontal and meso-scale variability, on the marine ecosystem. Detailed analysis of the results from the model and investigation of the biological variability with the climate change remain as future work. Two features; the difference in chl-a concentration between east and west in the subarctic North Pacific: the timing of spring bloom in the western subarctic gyre, especially interesting topics for further analysis. If the

marine ecosystem simulation using more fine resolution model is possible, the correct distribution of biological production can be demonstrated and is significantly contributed for this world.

## Acknowledgment

We thank Drs. Y. Masumoto, T. Kagimoto, and S. Kawahara for their collaborations in extending the OFES model for biological research. The QSCAT product of J-OFURO was obtained from Dr. Kutuwada. OFES simulations were conducted on the Earth Simulator under support of JAMSTEC.

(This article is reviewed by Dr. Julia Slingo.)

## References

[1] K. Banse, and D. C. English, Comparing phytoplankton seasonality in the eastern and western subarctic Pacific and the western Bering Sea, *Prog. Oceanogr*, vol.**43**, pp.235–288, 1999.

[2] K. Sasaoka, S. Saitoh, I. Asanuma, K. Imai, M. Honda, Y. Nojiri, and T. Saino, Temporal and spatial variability of chlorophyll-a in the western subarctic Pacific determined from satellite and ship observations from 1997 to 1999, *Deep-Sea Res. II*, vol.**49**, pp.5557–5576, 2002.

[3] J. I. Goes, K. Sasaoka, H. R. Gomes, S. Saitoh, and T. Saino, A Comparison of the seasonality and interannual variability of phytoplankton biomass and production in the western and wastern gyres of subarctic Pacific using multi-sensor satellite data, *J. Oceanogr*., vol.**60**, pp.75–91, 2004.

[4] A. Oschlies, W. Koeve, and V. Garçon, An eddy-permitting coupled physical-biological model of the North Atlantic: 2. Ecosystem dynamics and comparison with satellite and JGOFS local station data, *Global Biogeochem. Cycles*, vol.**14**, pp.499–523, 2000.

[5] A. Oschlies, Can eddies make ocean deserts bloom?, *Global Biogeochem. Cycles*, vol.**16**, 1106, doi:10.1029/2001GB001830, 2002.

[6] Y. Sasai, A. Ishida, H. Sasaki, S. Kawahara, H. Uehara, and Y. Yamanaka, A global eddy-resolving coupled physical and biological model: Physical influences on a marine ecosystem in the North Pacific, *Simulation*, vol.**82**, pp.467–474, 2006.

[7] A. Oschlies, and V. Garçon, An eddy-permitting coupled physical-biological model of the North Atlantic: 1. Sensitivity to advection numerics and mixed layer physics, *Global Biogochem. Cycles*, vol.**13**, pp.135–160, 1999.

[8] A. Oschlies, Model-derived estimates of new production: New results point towards lower values, *Deep-Sea Res. II*, vol.**48**, pp.2173–2197, 2001.

[9] H. Sasaki, Y. Sasai, M. Nonaka, Y. Masumoto, and S. Kawahara, An eddy-resolving simulation of quasi-global ocean driven by satellite-observed wind field, - Preliminary outcomes from physical and biological fields -, *J. Earth Simulator*, vol.**6**, pp.35–49, 2006.

[10] Y. Masumoto, H. Sasaki, T. Kagimoto, N. Komori, A. Ishida, Y. Sasai, T. Miyama, T. Motoi, H. Mitsudera, K. Takahashi, and H. Sakuma, A fifty-year-eddy-resolving simulation of the world ocean: Preliminary outcomes of OFES (OGCM for the Earth Simulator), *J. Earth Simulator*, vol.**1**, pp.35–56, 2004.

[11] R. C. Pacanowski, and S. M. Griffies, *MOM 3.0 Manual*, Geophysical Fluid Dynamics Laboratory/National Oceanic and Atmospheric Administration, 680pp, 2000.

[12] A. Rosati, and K. Miyakoda, A general circulation model for upper ocean circulation, *J. Phys. Oceanogr.*, vol.**18**, pp.1601–1626, 1988.

[13] E. Kalnay, M. Kanamitsu, R. Kistler et al., The NCEP/NCAR 40-year reanalysis project, *Bull. Am. Meteorol. Soc.*, vol.**77**, pp.437–471, 1996.

[14] M. Kubota, N. Iwasaka, S. Kizu et al., Japanese ocean flux data sets with use of remote sensing observations (J-OFURO), *J. Oceanogr*., vol.**58**, pp.213–225, 2002.

[15] K. Kutsuwada, Impact of wind/wind-stress field in the North Pacific constructed by ADEOS/NSCAT data, *J. Oceanogr*., vol.**54**, pp.443–456,1998.

[16] J. J. Polovina, E. A. Howel, D. R. Kobayashi, and M. P. Seki, The transition zone chlorophyll front, a dynamic global feature defining migration and forage habitat for marine resources, *Prog. Oceanogr.*, vol.**49**, pp.469–483, 2001.

[17] A. Shiomoto, and H. Asami, High-West and Low-East distribution patterns of chlorophyll a, primary productivity and diatoms in the subarctic North Pacific surface waters, midwinter 1996. *J. Oceanogr*., vol.**55**, pp.493–503, 1999.

[18] J. H. Martin, and R. M. Gordon, The case for iron, *Limnol. Oceanogr*, vol.**36**, pp.1793–1802, 1991.

[19] M. Nonaka, H. Hakamura, Y. Tanimoto, T. Kagimoto, and H. Sasaki, Decadal variability in the Kuroshio-Oyashio Etension simulated in an eddy-resolving OGCM, *J. Climate*, vol.**19**, pp.1970–1989, 2006.

[20] B. Taguchi, S.-P., Xie, N. Schnider, M. Nonaka, H. Sasaki, and Y. Sasai, Decadal variability of the Kuroshio Extension: Observations and an eddy-resolving model hidcast, *J. Climate*, Accepted, 2006.

[21] T. Kono, Modification of the Oyashio Water in the Hokkaido and Tohoku areas, *Deep-sea Res*., vol.**44**, pp.669–688, 1997.